Exome Sequencing Reveals a Novel *CWF19L1* Mutation Associated with Intellectual Disability and Cerebellar Atrophy

Christina Evers,[1]* Lilian Kaufmann,[1] Angelika Seitz,[2] Nagarajan Paramasivam,[3,4] Martin Granzow,[1] Stephanie Karch,[5] Christine Fischer,[1] Katrin Hinderhofer,[1] Georg Gdynia,[6,7] Michael Elsässer,[8] Stefan Pinkert,[9] Matthias Schlesner,[3] Claus R. Bartram,[1] and Ute Moog[1]

[1]Institute of Human Genetics, Heidelberg University, Heidelberg, Germany

[2]Department of Neuroradiology, University Hospital Heidelberg, Heidelberg, Germany

[3]Division of Theoretical Bioinformatics, German Cancer Research Center (DKFZ), Heidelberg, Germany

[4]Medical Faculty Heidelberg, Heidelberg University, Germany

[5]Center for Child and Adolescent Medicine, Pediatric Neurology, Heidelberg University Hospital, Heidelberg, Germany

[6]Institute of Pathology, University of Heidelberg, Heidelberg, Germany

[7]German Cancer Research Center, Clinical Cooperation Unit Molecular Tumor Pathology, Heidelberg, Germany

[8]Department of Obstetrics and Gynecology, Prenatal Medicine, University Hospital Heidelberg, Heidelberg, Germany

[9]Genomics and Proteomics Core Facility (GPCF), High Throughput Sequencing, German Cancer Research Center (DKFZ), Heidelberg, Germany

Intellectual disability (ID) with cerebellar ataxia comprises a genetically heterogeneous group of neurodevelopmental disorders. We identified a homozygous frameshift mutation in *CWF19L1* (c.467delC; p.(P156Hfs*33)) by a combination of linkage analysis and Whole Exome Sequencing in a consanguineous Turkish family with a 9-year-old boy affected by early onset cerebellar ataxia and mild ID. Serial MRI showed mildly progressive cerebellar atrophy. Absent C19L1 protein expression in lymphoblastoid cell lines strongly suggested that c.467delC is a disease-causing alteration. One further pregnancy of the mother had been terminated at 22 weeks of gestation because of a small cerebellum and agenesis of corpus callosum. The homozygous *CWF19L1* variant was also present in the fetus. Postmortem examination of the fetus in addition showed unilateral hexadactyly and vertebral malformations. These features have not been reported and may represent an expansion of the *CWF19L1*-related phenotypic spectrum, but could also be due to another, possibly autosomal recessive disorder. The exact function of the evolutionarily highly conserved C19L1 protein is unknown. So far, homozygous or compound heterozygous mutations in *CWF19L1* have been identified in two Turkish siblings and a Dutch girl, respectively, affected by cerebellar ataxia and ID. A zebrafish model showed that *CWF19L1* loss-of-function mutations result in abnormal cerebellar morphology and movement disorders. Our report corroborates that loss-of-function mutations in *CWF19L1* lead to early onset cerebellar ataxia and (progressive) cerebellar atrophy.

Key words: *CWF19L1*; ataxia; cerebellar atrophy; cerebellar hypoplasia; developmental delay; intellectual disability

How to Cite this Article:
Evers C, Kaufmann L, Seitz A, Paramasivam N, Granzow M, Karch S, Fischer C, Hinderhofer K, Gdynia G, Elsässer M, Pinkert S, Schlesner M, Bartram CR, Moog U. 2016. Exome sequencing reveals a novel *CWF19L1* mutation associated with intellectual disability and cerebellar atrophy.
Am J Med Genet Part A 170A:1502–1509.

INTRODUCTION

Hereditary cerebellar ataxias are a genetically and clinically heterogeneous group of disorders that can be associated with additional symptoms such as intellectual disability (ID). All patterns of inheritance have been described. In the majority, cerebellar ataxia with onset in childhood is of autosomal recessive inheritance. It can

Conflict of interest: none.
*Correspondence to:
Dr. Christina Evers, Institute of Human Genetics, Heidelberg University, Im Neuenheimer Feld 440, 69120 Heidelberg, Germany.
Email: christina.evers@med.uni-heidelberg.de

be caused by mutations in a multitude of genes (for review see Bird [1998] and Sailer and Houlden [2012]). The advent of next-generation sequencing technologies has facilitated the discovery of novel genes. Very recently, biallelic mutations in *CWF19L1* (complexed with cdc5 protein 19-like 1) were reported in two families with early onset cerebellar ataxia and cognitive impairment [Burns et al., 2014; Nguyen et al., 2016]. *CWF19L1* knockdown in a zebrafish model leads to abnormal cerebellar morphology and function [Burns et al., 2014]. We identified and characterized a novel homozygous frameshift mutation in *CWF19L1* in siblings, a boy and a female fetus, and report on associated clinical and neuroradiological findings.

MATERIALS AND METHODS

Patient Ascertainment

The affected boy and his parents were seen at the Outpatient Clinic of the Institute of Human Genetics, Heidelberg University, Germany. The affected fetus was seen at the Institute of Human Genetics and fetal autopsy was performed at the Institute of Pathology, Heidelberg University, Germany. The study adhered to the tenets of the Declaration of Helsinki and was approved by the local ethics committee. Informed consent was obtained from both parents.

DNA Isolation, Sanger Sequencing and cDNA Analysis

Genomic DNA was isolated from peripheral blood or skin fibroblast culture using a salting out procedure [Miller et al., 1988]. Exon 5 and adjacent intron boundaries of *CWF19L1* (RefSeq NM_018294.5) were sequenced using Big Dye Terminator V1.1 cycle sequencing kit and ABI 3130xl genetic analyzer. RNA was isolated form peripheral blood of the patient, his parents and healthy control persons as described previously [Chomczynski and Sacchi, 1987]. cDNA was synthesized through reverse transcription (RevertAid H Minus Reverse Transcriptase, Thermo Fisher Scientific, Inc.) according to the manufacturer's instructions. Different regions of the CWF19L1 transcripts were amplified by PCR (PhireII Hot Start DNA Polymerase, Thermo Fisher Scientific, Inc.) and analyzed on an agarose gel. Primer sequences and PCR conditions for Sanger sequencing and cDNA analysis are available upon request.

Array-Analysis/SNP Genotyping and Linkage Analysis

Affymetrix® Human Mapping 6.0 SNP array was performed as previously described [Evers et al., 2015] in order to genotype DNA of the affected boy, the fetus and both parents (I.1, I.2, II.4, and II.5, Fig. 1A) and to exclude genomic imbalances in the affected individuals (I.2 and I.3). Interpretation was based on human reference sequence GRCh37/hg19, February 2009. Genome-wide parametric linkage analysis with SNP genotypes was performed using ALOHOMORA and MERLIN software [Abecasis et al., 2002; Ruschendorf and Nurnberg, 2005], assuming affected family members were homozygous at a putative disease locus for an autosomal recessive disease allele inherited from a common ancestor. After performing several data quality checks, SNP marker with minor allele frequency (MAF) 0.15 and a minimum distance of 200,000 bp were selected to ensure low linkage disequilibrium between the markers.

Whole Exome Sequencing (WES)

WES was performed at the German Cancer Research Center (DKFZ), Heidelberg, on DNA of the affected boy (I.1) and both parents (II.4 and II.5) as previously described [Granzow et al., 2015]. Analysis of the sequence data was performed using the previously described Heidelberg exome data analysis bioinformatics pipeline [Granzow et al., 2015]. Shortly, raw reads were mapped to the hs37d5 (hg19 + decoy sequences) reference genome using BWA 0.6.2 [Li and Durbin, 2009] and PCR duplicates were marked by Picard (http://picard.sourceforge.net). SAMtools [Li et al., 2009] and Platypus [Rimmer et al., 2014] were used to call SNVs and indels, respectively, annotation was done using ANNOVAR [Wang et al., 2010]. Rareness of the variant in the population was measured using the MAF from Exome Aggregation Consortium (ExAC) database. Variants with greater than 1% MAF in this database were considered common alleles and removed from the candidate list. Using the ANNOVAR annotations, coding variants were defined as missense or nonsense mutations, indels overlapping exonic regions, and variants ±2 bases around the intron-exon junction. Variants ±2 bases around the intron-exon junction were considered splice-site variants.

Western Blot Analysis C19L1 in LCL Cells

Lymphoblastoid cell line (LCL) cells from patient II.1, his parents (II.4 and II.5) and healthy control persons were cultured as described previously [Hui-Yuen et al., 2011]. Protein was extracted from 5 ml culture using β-SH Sample buffer (Pepperkok Lab, EMBL, Heidelberg, Germany) and 15 µl of the protein lysate was separated by SDS-PAGE and blotted on a nitrocellulose membrane. Protein expression was analyzed on the western blot using commercially available antibodies targeting the C-terminal region of C19L1 (Anti-CWF19L1 HPA036890, Sigma–Aldrich, CWF19L1 Antibody PA5-31646, Life Technologies) and β-Actin (A5441, Sigma–Aldrich) as loading control.

RESULTS

Patient Reports

The first child, a boy (I.1, Fig. 1A), was born after 41 weeks of gestation. Birth weight (2,700 g, −2.3 SD), length (46 cm, −3.09 SD) and OFC (33 cm, −2.23 SD) were below the normal range. The parents were Turkish and third-degree cousins (II.3 and II.4, Fig. 1A). The boy sat without support at age 7 months and started to walk without support at 13 months. From the beginning he was walking unsteadily with frequent falling. He grew up bilingual (German and Turkish). At age 31 months he could speak only a few single words. On pediatric examination at age 3 years 10 months, a significant language delay was diagnosed;

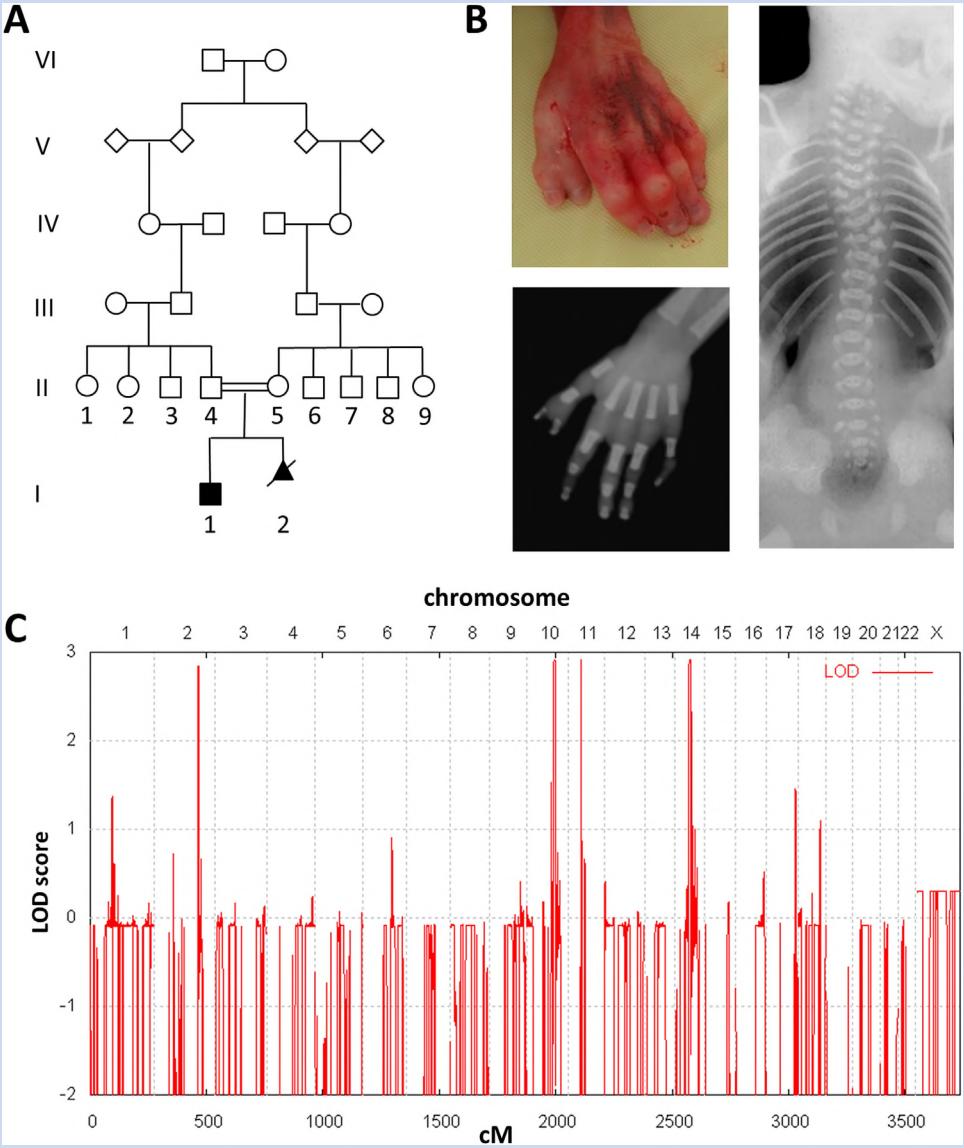

FIG. 1. (A) Pedigree of the family suggesting autosomal recessive inheritance due to male and female affected descendants and parents consanguinity. (B) Photograph and X-ray of the fetus left hand showing duplication of the terminal phalange of the thumb (left side of Fig. 1B). X-ray image of the spine demonstrating segmentation defects of the spine with hemivertebrae, butterfly vertebrae and scoliosis (rights side). (C) Linkage analysis: LOD-score distribution relative to chromosomal location with the highest LOD-score regions on chromosomes 2 (188.4–191.8 cM, corresponding to 18.4–19.2 Mbp), 10 (116.5–123.4 cM, 98.3–107.2 Mbp), 11 (56.1–56.5 cM, 38.4–39.5 Mbp), and 14 (62.1–69.9 cM, 63.1–71.9 Mbp) [Color figure can be seen in the online version of this article, available at http://wileyonlinelibrary.com/journal/ajmga].

speech was still limited to a few words. He showed unsteady, broad based gait, ataxic upper limb movements, intention tremor and dysarthria. While his height (97.5 cm, 7th centile) and weight (14.5 kg, 18th centile) corresponded to the low normal range, he was microcephalic (OFC 48 cm, −2.83 SD). Initial magnetic brain imaging (MRI) at age 3 years 11 months revealed isolated cerebellar atrophy, affecting the cerebellar vermis and hemispheres (Fig. 2A–D). Follow-up MRI at age 7 years and 8 months showed mildly progressive cerebellar atrophy. The third and last MRI performed 2 years later showed no further progression (Fig. 2E–H). He attended a special school for children with ID. At the age of 14 years, assessment with the Kaufman-Assessment Battery for Children (K-ABC), standardized for children up to 12.5 years, showed mild ID with a global "Mental Processing Scale" score of 57 (normal range 85–115), a "Sequential Scale" score of 56 and a "Simultaneous Scale" score of 57. Cognitive deficits were obvious in the "Nonverbal Scale" (global score: 52).

The boy was first seen at the Department of Human Genetics at age 9 years 10 months. He presented with gait ataxia, dysmetria, intention tremor and dysarthria. His height was 132 cm (7th centile),

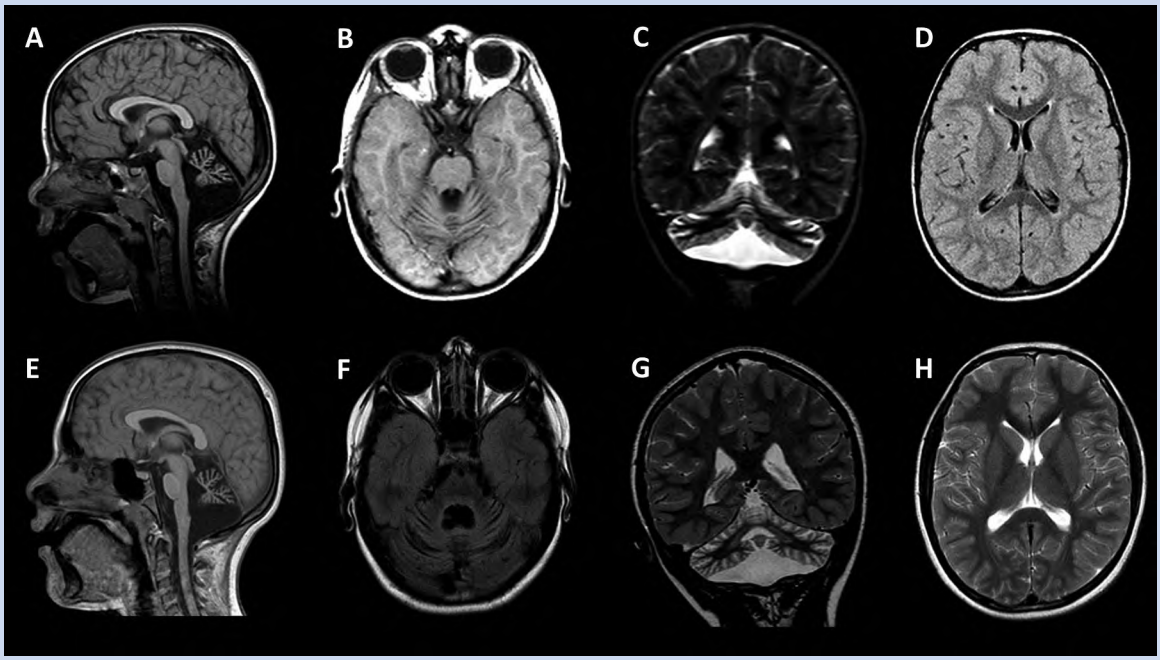

FIG. 2. MRI images of the affected boy (I.1) at age 3 years and 11 month (A–D) and 9 years and 9 month (E–H) showing cerebellar atrophy compared with those of a child with cerebellar hypoplasia (I–K). (A) Midline sagittal T1-weighted image showed thin cerebellar folia and prominent interfolial spaces affecting the entire cerebellum, but slightly more severe in the vermis. (B) Axial T1-weighted MRI demonstrated atrophy of cerebellar hemispheres and vermis. The cerebellar folia are thin with enlarged interfolial spaces. (C) Coronal T2-weighted image showed cerebellar atrophy of both hemispheres and the vermis with thin folia and prominent interfolial spaces. The vermis is slightly more affected than the hemispheres. (D) Supratentorial axial FLAIR image showed no abnormality. There was no evidence of supratentorial brain atrophy, supratentorial brain volume was normal. (E) Midline sagittal T1-weighted MRI showed mild progression of vermian atrophy. (F) Axial FLAIR image showed mild progression of the atrophy of the cerebellar hemispheres. (G) Coronal T2-weighted image showed mild progression of cerebellar atrophy affecting vermis and hemispheres. (H) Axial FLAIR at supratentorial level was still normal.

his weight 33.5 kg (50th centile), and OFC 51 cm (−2.15 SD). He had thick, bushy eyebrows and synophrys but no other dysmorphism. His parents characterized him as friendly and sociable.

In the second pregnancy, ultrasound examination at 16 weeks gestation was normal. Chromosome analysis after amniocentesis showed a normal female karyotype (46,XX, resolution of 400 bands). At 20 weeks ultrasound showed mild fetal ventriculomegaly, a transverse cerebellar diameter (TCD) in the low-normal range (18 mm, 8th centile) and normal cerebellar morphology. At 22 weeks a reduced TCD (18.6 mm, <1st centile) was detected by ultrasound. Fetal MRI at 22 weeks of pregnancy confirmed reduced TCD (18 mm, <1st centile) and mild ventriculomegaly (right ventricular diameter: 14 mm, left ventricular diameter: 11 cm). In addition, corpus callosum agenesis (CCA) was diagnosed. The pregnancy was terminated at 22 weeks of gestation. Autopsy showed a female fetus with a preauricular pit on the right side, duplication of the terminal phalange of the left thumb (Fig. 2B) and thoracic scoliosis. Fetal weight was 390 g (10th–25th centile), crown-to-heal-length was 27 cm (10th–25th centile). Fetal X-ray images confirmed preaxial hexadactyly and revealed segmentation anomalies of the thoracic spine with hemivertebrae, butterfly vertebrae and marked scoliosis (Fig. 2B). Detailed neuropathological examination was not possible due to autolysis.

Linkage Analysis

The four regions with the highest LOD (logarithm of the odds) score were localized on chromosome 2, 10, 11, and 14 (maximal LOD scores of 2.85, 2.91, 2.91, and 2.91, respectively) (Fig. 1C). Another six regions showed LOD scores of more than 1.0. A summary of all ten regions with LOD scores of more than 1.0. is given in Supplemental Table S1.

Whole Exome Sequencing and Sanger Sequencing

On average 98.323% of bases in the target regions had at least 10× coverage with a median-of-median base coverage of 89×. Only non-synonymous single nucleotide variants (SNVs) resulting in a stop codon, loss of a stop codon or in a codon that codes for a different amino acid, splice site variants and indels in or near exons with MAF ≤1% were considered. A total of 10 variants were identified which were homozygous in the index patient and heterozygous in the parents and therefore consistent with autosomal recessive inheritance in a consanguineous family (Supplemental Table S2).

Only the variant in *CWF19L1* was located in one of the genomic regions with maximal LOD-scores (Supplemental Table S1).

It is located within an 8.8 Mb linkage region on chromosome 10 with maximal LOD score of 2.91 (Fig. 1C, Supplemental Table S1). This *CWF19L1* variant c.467delC; p.(P156Hfs*33) (RefSeq NM_018294.5) is predicted to result in a frameshift at codon 156 with the introduction of 33 missense amino acids followed by a premature stop at codon 189 (Fig. 3C). It is absent in the 1,000 genome project [Abecasis et al., 2012], in the EVS (http://evs.gs.washington.edu) and the ExAC database. The variant in *CWF19L1* is the only one of the ten filtered variants that is located in a gene that has already been described to be associated with a similar human phenotype, namely cerebellar ataxia and ID [Burns et al., 2014]. Therefore, the *CWF19L1* frameshift variant was considered possibly pathogenic and further assessed. It was confirmed by Sanger sequencing in the affected patient (I.1), and also found homozygous in the affected fetus (I.2). Both parents were found to be heterozygous carriers (Fig. 3A).

All other nine variants were not located within the linkage regions (Supplemental Table S1). Eight variants were non-synonymous SNVs (in the genes *FLG*, *ZBED6*, *DRD1*, *SSH1*, *LPIN2*, *KIAA0355*, *BPIFB6*, *DLGAP4*). The variant in *MYO7*, a gene coding for a myosin protein, was predicted to result in a loss of the stop codon. It was excluded from further considerations because it was also present in a local control in-house database [Granzow et al., 2015] and because mutations in this gene lead to Usher syndrome 1B which is characterized by deafness, reduced vestibular function, and retinal degeneration. The eight non-synonymous SNVs were further assessed by seven different variant effect prediction tools (SIFT [Ng and Henikoff, 2003], PolyPhen2 [Adzhubei et al., 2010], LRT [Chun and Fay, 2009], MutationTaster [Schwarz et al., 2010], MutationAssessor [Reva et al., 2011], FATHMM [Shihab et al., 2013], and PROVEAN [Choi et al., 2012]) from dbNSFP v2.0 [Liu et al., 2013]. Two variants (in *DRD1* and *BPIFB6*) were consistently classified as benign. Ambiguous results were obtained for the variants in *FLG*, *ZBED6*, *SSH1*, *LPIN2*, *KIAA0355*, *DLGAP4*. Mutations in *FLG* and *LPIN2* were described as causative for a different phenotype (ichthyosis vulgaris and recurrent multifocal osteomyelitis with congenital dyserythropoietic anemia [Majeed syndrome], respectively). No human phenotype for *ZBED6*, *SSH1*, *KIAA0355*, *DLGAP4*, and *HRC* mutation carriers has been described. Of these genes, only *DLGAP4* has a putative role in the human brain. The product of this gene is a membrane-associated guanylate kinase found at the post-synaptic density in neuronal cells. However, only MutationTaster predicted a disease causing effect of this variant.

RNA and Protein Analyses

cDNA of three different regions of *CWF19L1* could be amplified in the affected boy I.2 (exons 3–4, 5–7, and 11–12, Fig. 3D), showing that *CWF19L1* mRNA was not entirely degraded by nonsense-mediated mRNA decay (NMD). It is expected that the *CWF19L1* frameshift mutation results in a premature termination of translation and in the synthesis of a truncated protein lacking the last 349 amino acids. Analysis of C19L1 protein expression using two antibodies targeting the C-terminus of C19L1 on cell extracts of LCL cells derived from the patient and his parents revealed that C19L1 is not detectable in the patient, but in his parents and controls. Fig. 3E shows a representative result using antibody HPA036890 (Sigma), which was more sensitive and specific than the antibody PA5-31646 (Life Technologies). This antibody detected the full length C19L1 isoform 1 (61 kDa) which is missing in the patient, and a weak band at about 33 kDa which corresponds to the expected size of isoform 4 (Fig. 3E). However, the intensity of the putative C19L1 isoform 4 protein band is similar in the patient, his parents and controls and there is no evidence for an increased translation of isoform 4 from the alternative start codon in exon 8 downstream of the mutation in the patients LCLs. Bands corresponding to the other putative isoforms 2 (56 kDa) and 3 (46 kDa) could not be detected (arrows in Fig. 3E), albeit two further bands at 39 kDa and 16 kDa are considered to be not specific (asterisces in Fig. 3E). In summary, our analyses indicate that the full-length C19L1 protein is not expressed in the patient.

DISCUSSION

We present a detailed clinical, neuroradiological and molecular description of a boy and a female fetus from a consanguineous Turkish family with a novel homozygous *CWF19L1* frameshift mutation identified by linkage analysis and WES. The patients in this report and the individuals reported previously [Burns et al., 2014; Nguyen et al., 2016] a showed cerebellar ataxia. Mild ID was an additional feature in one siblings described by Burns et al. [2014], the patient of Nguyen et al. [2016] and in our male patient. The IQ of the other sibling reported by Burns et al. [2014] was within the normal range (IQ 90).

Further characterization of the frameshift *CWF19L1* variant c.467delC indicates a loss-of-function mechanism: the variant introduces a premature stop codon at amino acid 189 (p.(P156Hfs*33)). *CWF19L1* mRNA in our patient was not completely degraded by NMD. We therefore expected the synthesis of a truncated C19L1 protein lacking the last 349 amino acids (Fig. 3C). Using antibodies against the c-terminus of the C19L1 protein we could neither detect the full length protein (isoform 1) nor a change in expression of other putative isoforms of C19L1 generated by the alternative start codons (Fig. 3B) in the patients LCLs, suggesting that there is no increased translation of these other isoforms to compensate for the loss in the patient. The truncated protein generated by the default start codon would consist of the N-terminus of C19L1 and hence was not targeted by the antibodies used. We did not address whether it is expressed or subjected to instant proteasomal degradation. Since it would be lacking large parts and essential domains of the protein and we assume that it would not be functional.

The full-length C19L1 protein contains 538 amino acids and is predicted to contain a metallophosphatase (MMP) domain, a histidine triad motif (HIT) domain and a C-terminal Cwf-J-C domain (Fig. 3C). The predicted truncated protein product due to the nonsense mutation p.(P156Hfs*33) lacks nearly two thirds of its c-terminal part (Fig. 3C). Interestingly, the c-terminal region of human C19L1 is found in the N-terminus of the yeast protein CwfJ, which is part of the Cdc5p protein complex involved in mRNA splicing and cell-cycle-control/arrest [Ohi et al., 2002; Stelzl et al., 2005; Ren et al., 2011]. Both, the mutation found in our patient and the stop mutation of the girl reported by

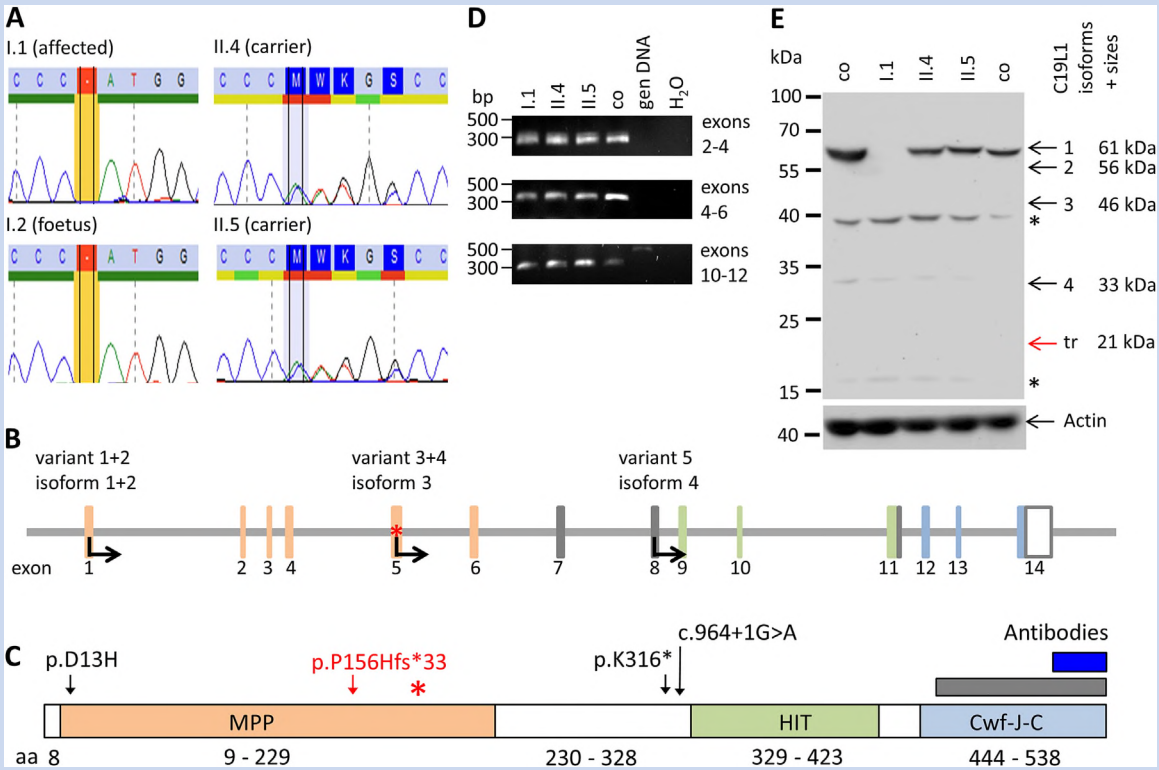

FIG. 3. (A) Sequence analysis by Sanger sequencing showed homozygosity for the frameshift mutation c.467delC; p.(P156Hfs*33) in Exon 5 of *CWF19L1* in the affected boy (I.1) and fetus (I:2) and heterozygosity in the healthy parents (II.4 and II.5). (B) Schematic exon/intron structure of *CWF19L1*. Exon are shown as vertical bars and numbered below according to ensemble transcript ENST00000354105 (http://www.ensemble.org, which corresponds to RefSeq NM_018294.5). The color-coding of the exons reflects the domains of the protein shown in (C), unstructured domains are marked in grey and the 3′UTR in exon 14 is highlighted by a white box. Bent arrows at the bottom of the exons indicate the three alternative start codons of the five different known transcript variants (variant 1 = NM_018294.5, variant 2 = NM_001303404.1, variant 3 = NM_001303405.1, variant 4 = NM_001303406.1, variant 5 = NM_001303407.1) which result in 4 different protein isoforms. Compared to the full length C19L1 (isoform 1), isoform 2 is missing exon 12 and therefore a part within the CWF-J-C domain, isoform 3 is missing a large N-terminal part of the MPP domain and isoform 4 only comprises the HIT and CWF-J-C domain. The novel mutation c.467delC leads to putative premature stop codon (marked by an asterisk), which occurs after the alternative start codon in exon 5. (C) Predicted protein domain structure of C19L1. The 538 amino acid full-length protein is predicted to contain a metallophosphatase (MMP) domain (orange), a histidine triad motif (HIT) domain (green) and a C-terminal Cwf-J-C domain (blue). Below numbering of amino acids (aa) is given. The novel mutation c.467delC leads to a frameshift starting at amino acid 156 (shown by a red arrow) which results in a putative premature stop codon at amino acid 189 (marked by an red asterisk). The location of the mutations reported by Burns et al. [2014] and Nguyen et al. [2016] is indicated by black arrows. The c-terminal parts of C19L1 against which the antibodies are raised are indicated by a blue or grey box (antibodies HPA036890 and PA5-31646, respectively). (D) cDNA analysis of CWF19L1. Amplification of exons 2–4, 4–6, and 10–12 of CWF19L1 cDNA of the affected homozygous boy (I.1), the healthy heterozygous parents (II.4 and II.5) and a healthy control person (control) and of genomic DNA of a healthy control person (gen. DNA). Corresponding sizes of a DNA ladder (Thermo Fisher, 100 bp Plus) are indicated on the left. (E) Protein expression analysis of LCL cells of the patient (I.1), his parents (II.4 and II.5) and control persons (co) using the anti-C19L1 antibody HPA036890 targeting the c-terminus and an anti-actin antibody as loading control. Arrows indicate the size of the (predicted) C19L1 protein isoforms. Molecular weights were calculated by ExPASy server (http://web.expasy.org/compute_pi/). The full length protein (isoform 1) has a size of 61 kDa [Burns et al., 2014] and is indicated by a black arrow. The isoforms 2, 3, and 4 have a prediced size of 56, 46, and 33 kDa (black arrows), the predicted truncated protein p.(P156Hfs*33) has a size of 21 kDa (red arrow). Non-specific bands that are unchanged in the patient are marked by an asterisk. The protein standard (ps) and the sizes (kDa) are indicated on the left [Color figure can be seen in the online version of this article, available at http://wileyonlinelibrary.com/journal/ajmga].

Nguyen et al. [2016], lead to a truncated protein lacking the c-terminus. Aberrant splicing, which is involved in several neurological human diseases [Feng and Xie, 2013], could be a putative pathomechanism. It is possible that *CWF19L1* is in a line with other genes for neurological diseases involved in basic cellular processes such as mRNA splicing [Kalscheuer et al., 2003; Feng and Xie, 2013; Mizuguchi et al., 2014].

However, there are several open questions. First, the female fetus had additional anomalies (CCA, duplication of the terminal phalange of the right thumb, thoracic hemivertebrae, scoliosis and

preauricular pit). A causal link between the *CWF19L1* variant and these additional findings of the fetus is not evident. It remains unclear whether these malformations are part of the phenotypic spectrum of *CWF19L1* mutations and have reduced penetrance, or if they have another cause. Further genetic analysis of the fetus, for example, by WES, was not possible due to limited amounts of fetal DNA. Second, the MRI findings of the family reported by Burns et al. [2014] were described as hypoplasia of cerebellar vermis and hemispheres, whereas serial MRIs in our male patient showed slightly progressive cerebellar atrophy (Fig. 2A–H). Nguyen et al. [2016] used the terms cerebellar atrophy and hypoplasia inconsistently to describe mild progression of decrease in the cerebellar vermis and hemisphere volume in their patient [Nguyen et al., 2016]. The MRIs of the siblings described by Burns et al. [2014] have been previously published [Yapici and Eraksoy, 2005]. Axial and sagittal T1-weighted MRI images showed massively enlarged interfolial spaces in both children. This cerebellar morphology was also found in the patient of Nguyen et al. [2016] and the present patient. According to Barkovich [2005] it is more characteristic for cerebellar atrophy than hypoplasia. It seems that *CWF19L1* mutations are associated with cerebellar atrophy, rather than cerebellar hypoplasia. The early onset ataxia in all patients and the prenatally reduced TCD in the described fetus could indicate prenatal onset of cerebellar atrophy. Alternatively, cerebellar atrophy may have superimposed on hypoplasia which is difficult to diagnose [Poretti et al., 2014]. Due to inaccuracy of ultrasound and MRI measurements before the gestational age of 24 weeks definitive conclusions cannot be drawn.

In conclusion, our findings provide further evidence that *CWF19L1*, coding for a protein with a predicted role in mRNA processing, is a novel gene for autosomal recessive ataxia with early onset, mildly progressive cerebellar atrophy and ID.

ACKNOWLEDGMENTS

We thank Susanne Theiß and Karin Hüllen for their outstanding technical assistance and Jens-Peter Schenk for providing fetal radiographs. We are very grateful to the family who contributed to this study.

REFERENCES

Abecasis GR, Auton A, Brooks LD, DePristo MA, Durbin RM, Handsaker RE, Kang HM, Marth GT, McVean GA. 2012. An integrated map of genetic variation from 1,092 human genomes. Nature 491:56–65.

Abecasis GR, Cherny SS, Cookson WO, Cardon LR. 2002. Merlin-rapid analysis of dense genetic maps using sparse gene flow trees. Nat Genet 30:97–101.

Adzhubei IA, Schmidt S, Peshkin L, Ramensky VE, Gerasimova A, Bork P, Kondrashov AS, Sunyaev SR. 2010. A method and server for predicting damaging missense mutations. Nat Methods 7:248–249.

Barkovich AJ. 2005. Differentiation of cerebellar atrophy from hypoplasia. In: Barkovich AJ, editor. Pediatric neuroimaging. 4e. Philadelphia: Lippincott Williams & Wilkins. pp 165–167.

Bird TD. 1998. Hereditary ataxia overview. In: Pagon RA, Adam MP, Ardinger HH, Wallace SE, Amemiya A, Bean LJH, Bird TD, Fong CT, Mefford HC, Smith RJH, Stephens K, editors. GeneReviews. Seattle: University of Washington. [updated 2015 Jun 11] Available from http://www.ncbi.nlm.nih.gov/books/NBK1138/

Burns R, Majczenko K, Xu J, Peng W, Yapici Z, Dowling JJ, Li JZ, Burmeister M. 2014. Homozygous splice mutation in *CWF19L1* in a Turkish family with recessive ataxia syndrome. Neurology 83:2175–2182.

Choi Y, Sims GE, Murphy S, Miller JR, Chan AP. 2012. Predicting the functional effect of amino acid substitutions and indels. PLoS ONE 7: e46688.

Chomczynski P, Sacchi N. 1987. Single-step method of RNA isolation by acid guanidinium thiocyanate-phenol-chloroform extraction. Anal Biochem 162:156–159.

Chun S, Fay JC. 2009. Identification of deleterious mutations within three human genomes. Genome Res 19:1553–1561.

Evers C, Paramasivam N, Hinderhofer K, Fischer C, Granzow M, Schmidt-Bacher A, Eils R, Steinbeisser H, Schlesner M, Moog U. 2015. SIPA1L3 identified by linkage analysis and whole-exome sequencing as a novel gene for autosomal recessive congenital cataract. Eur J Hum Genet 23:1627–1633.

Feng D, Xie J. 2013. Aberrant splicing in neurological diseases. Wiley Interdiscip Rev RNA 4:631–649.

Granzow M, Paramasivam N, Hinderhofer K, Fischer C, Chotewutmontri S, Kaufmann L, Evers C, Kotzaeridou U, Rohrschneider K, Schlesner M, Sturm M, Pinkert S, Eils R, Bartram CR, Bauer P, Moog U. 2015. Loss of function of PGAP1 as a cause of severe encephalopathy identified by Whole Exome Sequencing: Lessons of the bioinformatics pipeline. Mol Cell Probes 29:323–329.

Hui-Yuen J, McAllister S, Koganti S, Hill E, Bhaduri-McIntosh S. 2011. Establishment of Epstein-Barr virus growth-transformed lymphoblastoid cell lines. J Vis Exp 57:3321.

Kalscheuer VM, Freude K, Musante L, Jensen LR, Yntema HG, Gecz J, Sefiani A, Hoffmann K, Moser B, Haas S, Gurok U, Haesler S, Aranda B, Nshedjan A, Tzschach A, Hartmann N, Roloff TC, Shoichet S, Hagens O, Tao J, Van Bokhoven H, Turner G, Chelly J, Moraine C, Fryns JP, Nuber U, Hoeltzenbein M, Scharff C, Scherthan H, Lenzner S, Hamel BC, Schweiger S, Ropers HH. 2003. Mutations in the polyglutamine binding protein 1 gene cause X-linked mental retardation. Nat Genet 35:313–315.

Li H, Durbin R. 2009. Fast and accurate short read alignment with Burrows-Wheeler transform. Bioinformatics 25:1754–1760.

Li H, Handsaker B, Wysoker A, Fennell T, Ruan J, Homer N, Marth G, Abecasis G, Durbin R, Genome Project Data Processing S. 2009. The sequence Alignment/Map format and SAMtools. Bioinformatics 25:2078–2079.

Liu X, Jian X, Boerwinkle E. 2013. DbNSFP v2.0: A database of human non-synonymous SNVs and their functional predictions and annotations. Hum Mutat 34:E2393–E2402.

Miller SA, Dykes DD, Polesky HF. 1988. A simple salting out procedure for extracting DNA from human nucleated cells. Nucleic Acids Res 16:1215.

Mizuguchi M, Obita T, Serita T, Kojima R, Nabeshima Y, Okazawa H. 2014. Mutations in the PQBP1 gene prevent its interaction with the spliceosomal protein U5-15 kD. Nat Commun 5:3822.

Ng PC, Henikoff S. 2003. SIFT: Predicting amino acid changes that affect protein function. Nucleic Acids Res 31:3812–3814.

Nguyen M, Boesten I, Hellebrekers DM, Vanoevelen J, Kamps R, de Koning B, de Coo IF, Gerards M, Smeets HJ. 2016. Pathogenic CWF19L1 variants as a novel cause of autosomal recessive cerebellar ataxia and atrophy. Eur J Hum Genet 24:619–622.

Ohi MD, Link AJ, Ren L, Jennings JL, McDonald WH, Gould KL. 2002. Proteomics analysis reveals stable multiprotein complexes in both fission and budding yeasts containing Myb-related Cdc5p/Cef1p, novel pre-mRNA splicing factors, and snRNAs. Mol Cell Biol 22:2011–2024.

Poretti A, Boltshauser E, Doherty D. 2014. Cerebellar hypoplasia: Differential diagnosis and diagnostic approach. Am J Med Genet Part C Semin Med Genet 166C:211–226.

Ren L, McLean JR, Hazbun TR, Fields S, Vander Kooi C, Ohi MD, Gould KL. 2011. Systematic two-hybrid and comparative proteomic analyses reveal novel yeast pre-mRNA splicing factors connected to Prp19. PLoS ONE 6:e16719.

Reva B, Antipin Y, Sander C. 2011. Predicting the functional impact of protein mutations: Application to cancer genomics. Nucleic Acids Res 39:e118.

Rimmer A, Phan H, Mathieson I, Iqbal Z, Twigg SR, Consortium WGS, Wilkie AO, McVean G, Lunter G. 2014. Integrating mapping-, assembly- and haplotype-based approaches for calling variants in clinical sequencing applications. Nat Genet 46:912–918.

Ruschendorf F, Nurnberg P. 2005. ALOHOMORA: A tool for linkage analysis using 10K SNP array data. Bioinformatics 21:2123–2125.

Sailer A, Houlden H. 2012. Recent advances in the genetics of cerebellar ataxias. Curr Neurol Neurosci Rep 12:227–236.

Schwarz JM, Rodelsperger C, Schuelke M, Seelow D. 2010. MutationTaster evaluates disease-causing potential of sequence alterations. Nat Methods 7:575–576.

Shihab HA, Gough J, Cooper DN, Stenson PD, Barker GL, Edwards KJ, Day IN, Gaunt TR. 2013. Predicting the functional, molecular, and phenotypic consequences of amino acid substitutions using hidden Markov models. Hum Mutat 34:57–65.

Stelzl U, Worm U, Lalowski M, Haenig C, Brembeck FH, Goehler H, Stroedicke M, Zenkner M, Schoenherr A, Koeppen S, Timm J, Mintzlaff S, Abraham C, Bock N, Kietzmann S, Goedde A, Toksoz E, Droege A, Krobitsch S, Korn B, Birchmeier W, Lehrach H, Wanker EE. 2005. A human protein-protein interaction network: A resource for annotating the proteome. Cell 122:957–968.

Wang K, Li M, Hakonarson H. 2010. ANNOVAR: Functional annotation of genetic variants from high-throughput sequencing data. Nucleic Acids Res 38:e164.

Yapici Z, Eraksoy M. 2005. Non-progressive congenital ataxia with cerebellar hypoplasia in three families. Acta Paediatr 94:248–253.

SUPPORTING INFORMATION

Additional supporting information may be found in the online version of this article at the publisher's web-site.